

Solid state dye-sensitized solar cells based on barium strontium titanate nanorod film

Mohsen Safaei¹, Thamir Hassen Ali², Odai N. Salman³, Mukhlis M. Ismail^{3*} ,
Ling Shing Wong⁴, Mohd. Hashim⁵, Ateeq Ahmed⁶

¹ Division of Dental Biomaterials, School of Dentistry, Kermanshah University of Medical Sciences, Kermanshah, Iran

² Middle Technical University- Electrical Engineering Technical College, Baghdad, Iraq

³ Department of Applied Science, University of Technology, Iraq

⁴ Faculty of Health and Life Sciences, INTI International University, Nilai, 71800 Malaysia

⁵ Department of Applied Physics, Aligarh Muslim University, Aligarh 202002, India

⁶ Department of Materials Science and Engineering, Chosun University, South Korea

* Corresponding author's e-mail: mmismail009@gmail.com

ABSTRACT

Perovskite barium strontium titanate ($\text{Ba}_{0.7}\text{Sr}_{0.3}\text{TiO}_3$ – BST) nanorod film was effectively produced and characterized. TiO_2 nanorods were prepared hydrothermally; after that they were deposited on an fluorine tin-oxide (FTO) substrate at 150 °C for 4 h. X-ray diffraction (XRD) showed that the $\text{Ba}_{0.7}\text{Sr}_{0.3}\text{TiO}_3$ film was polycrystalline with a low trace of peaks that belonged to TiO_2 , indicating that the BST films needed more reaction time. According to the optical properties, the band gap of the BST nanorod film was 3.16 eV, and strong photoluminescence centered at 367 nm. The data from the BST film can be used to calculate the energy gap. A direct electric current conductivity measurement showed that it increases along with temperature up to the Curie temperature, and the behavior was the opposite. Photoelectrode properties like open circuit voltage, short circuit photocurrent density, fill factor, and efficiency have been measured. The efficiency was 0.071 when preparing solid-state dye-sensitized solar cells based on BST film.

Keywords: perovskite, solid-state dye-sensitized solar cell, reflection spectra, hydrothermal technique.

INTRODUCTION

In a wide range of applications, ferroelectrics are key ingredients and barium strontium titanate (BST) is one of them [1–5]. The material is an exemplary ABO_3 perovskite structure of numerous features, such as high dielectric constant, good stability, low current leakage [6–9], low dissipation factor [10], low optical losses [11], and composition-dependent Curie temperatures [12]. Because the replacement of Sr^+ for Ba^+ in the BST lattice may shift the T_c to lower temperatures, the ferroelectric/paraelectric phase transition temperature (T_c) may be adjusted by changing the Ba/Sr ratio [13]. The ideal perovskite structure features a cubic unit cell with a side of approximately 3.9Å,

a space group of Pm3m. The oxygen coordination of the B ions is octahedral, whereas the oxygen coordination of the A ions is 12-fold. Six cations ($4A + 2B$) are connected to the oxygen ions. If the unit cell is chosen with a B ion at the body center, the oxygen ions fill the face centers of the unit cell and the A ions occupy its corners. The oxygen ions are in the middle of the edges and the B ions are at the entrances of unit cells when the A ion is allocated the body center location [14]. The most experimentally and theoretically inspected ferroelectric material is barium strontium titanate ($\text{Ba}_{1-x}\text{Sr}_x\text{TiO}_3$) due to it is a preliminary ferroelectric, utilized widely as [15], voltage-tunable capacitors [16], actuators [17], solar cells [18], oscillators [19], light detector [20] and optical, acoustic

devices [21]. $\text{Ba}_{1-x}\text{Sr}_x\text{TiO}_3$ is a continuous solid solution between two conventional ferroelectrics barium titanate (BaTiO_3) and strontium titanate (SrTiO_3). BST is a nonconductor at ambient temperature due to the large value of the energy band gap [22] and also has been investigated in bulk, glass-ceramic and thin film forms [23]. BST is a perovskite structural material that is ecologically benign [24]. Numerous discoveries made by many academics in recent years have been linked to the use of renewable energy technology. A solar cell is an electronic device that transforms photons from the Sun's energy directly into electrical energy. The photovoltaic effect is the name given to this conversion process. Due to their widespread availability, many ferroelectric materials can be used in solar cell applications. BaTiO_3 , SrTiO_3 , and BST are some of the ferroelectric minerals that are accessible for use in solar cell applications [25]. Furthermore, by changing the barium-to-strontium ratio, the temperature range in which the ferroelectric behavior is reflected may be readily adjusted [26]. BST is a ferroelectric material, as it represents a unique class of crystalline materials in which the electric polarization appears automatically, which helps to form specific regions divergent from each other, determined by the direction of the electric dipoles and separated from each other by walls in which these dipoles are gradually changed. Small polarizing regions play an essential role in forming an internal constructive potential employed in dye-stained solar cells. Many effective and efficient techniques have been devoted to the synthesis of new morphologies of BT and BST in past research, including solid-state reaction [27] sol-gel [28], Pulse laser deposition [29], chemical vapor deposition [30], spray pyrolysis [31], hydrothermal process [23], and the features of the hydrothermal technique involve the ease, low cost, and homogeneity of the product, with an uncomplicated aggregation method at comparatively low temperatures [32]. Energy harvesting techniques are still a major concern to take advantage of the existing energies. One of the most important features of solar cells is that they have the ability to convert light into electricity even in the presence of weak lighting with low efficiency. Therefore, the researchers' attention turned to increasing the efficiency of the solar cell, even under weak lighting. The effect of duration time on the size and structure of crystalline TiO_2 has been investigated by many researchers, such as Zhao et al. [33]. TiO_2 films

with thicknesses ranging from 0.7 to 2.3 μm were produced and placed on FTO substrates for use as electrodes in DSSC [34]. They discovered that increasing the thickness of TiO_2 films improves dye adsorption via TiO_2 layers as well as V_{oc} and I_{sc} . Chen et al. [35] studied alkaline metal halide Perovskites, inorganic oxide perovskites, and organic metal halide perovskites. Dewi [36] study the variations in Sr of $\text{Ba}_{1-x}\text{Sr}_x\text{TiO}_3$ thin film that grown on a glass substrate, which has been carried out using the sol-gel method. He showed that the composition is greatly influence absorbance. The higher the Sr composition in the thin film, the lower the absorbance produced. The width of the energy band-gap obtained from the $\text{Ba}_{1-x}\text{Sr}_x\text{TiO}_3$ ($x = 0.25: 0.3$ and 0.35) thin film was determined using the Tauc Plot method and the energy band-gap of $\text{Ba}_{0.75}\text{Sr}_{0.25}\text{TiO}_3$. In this paper, the authors focused on the synthesis of barium strontium titanate ($\text{Ba}_{0.7}\text{Sr}_{0.3}\text{TiO}_3$) utilizing hydrothermally treated TiO_2 nanorods films of various thicknesses has been effectively accomplished in this work for use in solid-state dye-sensitized solar cells. In the current research, a ferroelectric material (BST) was used in a dye-sensitized solar cell after preparing it in the form of a film, using the hydrothermal method. The surface area of the ferroelectric film was increased by controlling the preparation mechanism and a nanorod film was obtained. The efficiency of the making solid-state dye-sensitized solar cell was measured.

EXPERIMENTAL

Synthesis of barium strontium titanate thin films

The formation of BST films with different morphology and structure is twofold: firstly, the growth of the titanium dioxide films vertically on the fluorine tin-oxide (FTO) substrate utilizing the hydrothermal technique. FTO substrates were washed using isopropanol, acetone, and deionized water (DW) before being ultrasonically cleaned for 45 min and after that, the samples were rinsed with deionized water. TiO_2 nanorods were made by mixing an equal volume of 30 mL deionized water and hydrochloric acid in concentrated form, after that stirring until 25 min then titanium butoxide (1 mL) was added. The result was poured into a Teflon-lined stainless steel autoclave, after placing the samples at an angle against the Teflon

container with the conducting side facing down at 150 °C for 4 h. After synthesis, the autoclave was cooled at ambient temperature and the samples were taken out and rinsed carefully with deionized water. Secondly, an appropriate amount of barium and strontium hydroxides was dissolved and still stirred for 120 minutes on a hotplate at 80 °C until formed transparent solution was. Subsequently, the mixed solution was poured into a 100 ml Teflon-lined autoclave where TiO₂ substrate is inside it. The hydrothermal process was conducted at 150 °C for 2 hours to produce BST film, then was cooling and rinsing process is done with acetone. Finally, the BST films were dried at room temperature. After that, the BST nanorods were annealed for half an hour at 450 °C in the air. Then, the BST film has been dyed by immersing it in N719 (0.25 mM) dye solution for 24 h to be the absorber. The Spiro-OMeTAD hole-transporter layer (HTM) was deposited on BST film by spin coating (2000 r.p.m. for 60 s) after dissolving 60 µL of spiro-OMeTAD in 1 ml of chlorobenzene solution at room temperature. The hole-transport layer (HTL) was diffused onto the surface of the BST. Finally, the gold thin film was deposited on HTL by thermal evaporation technique (Edward 306 England equipment at 2×10^{-5} mbar). Figure 1 illustrates the structure of ss-DSSC structure.

The structure of prepared films was examined using the X-ray diffraction (XRD) model (Shimadzu XRD 6000), Cu K α radiation ($\lambda = 1.5406 \text{ \AA}$), 40 kV and 30 mA at a 1° scanning speed in the 2 θ range from 20° to 80° was used to investigate the crystal phase and chemical composition. An ultraviolet spectrophotometer (UV–Vis) is used to study the optical properties. The recombination rates of charge transfer were examined, where 277 nm have been excited using a fluorescence spectrophotometer. BST nanorod films were measured by diffuse reflectance spectra; furthermore, the optical properties examined

by photoluminescence (PL), besides the electrical properties of the fabricated samples, were examined. The ss-DSSCs were characterized using a variety of key characteristics. The BST film that was produced served as a bridge between the p-type (Spiro-OMeTAD) and n-type. On a BST substrate, the Spiro-OMeTAD solution was developed. This link was created during the spin coating process, to be precise. Using a thermal evaporation deposition system, gold was deposited on Spiro-OMeTAD and FTO to create the electrodes. The ss-DSSC measurements were performed with a Xenon lamp and TES 1333R solar power meter to produce 100 mW/cm².

RESULTS AND DISCUSSION

The X-ray diffraction of TiO₂ and Ba_{0.7}Sr_{0.3}TiO₃ samples deposited on FTO substrate through hydrothermal technique at 150 °C for 2 h is shown in Figure 2. The TiO₂ film deposited on FTO is rutile, as shown in Figure 2, where the pattern peaks were in well compatible with the tetragonal rutile TiO₂ peaks (JCPDS no.21-1276). Figure 2 also shows the appearance of FTO peaks (SnO₂). The rutile TiO₂ transformed to the BST phase after being hydrothermally treated as shown in Figure 2. It is also indicated that the BST film has good crystallinity and is compatible with ferroelectric tetragonal phase distinct peaks are similar to that reported by Joshi et al. [37]. Peaks are assigned by comparing the observed peaks to the standard JCPDS card no. 39–1395. The BST peaks in all specimens primarily grow along (100) orientations [38, 39]. Table 1 summarizes the matching XRD result. The results of Figure 2 also showed that the value of the lattice constants *a* and *b* was 0.366 nm and *c* was 0.376 nm respectively, the lattice constants was pointed to the congruously tetragonal phase. The crystallite size (*D*) was

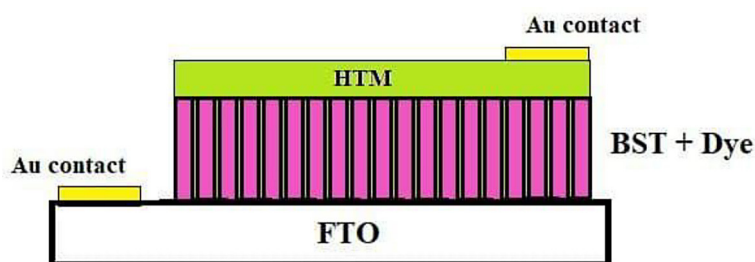


Figure 1. Solid state dye-sensitized solar cell

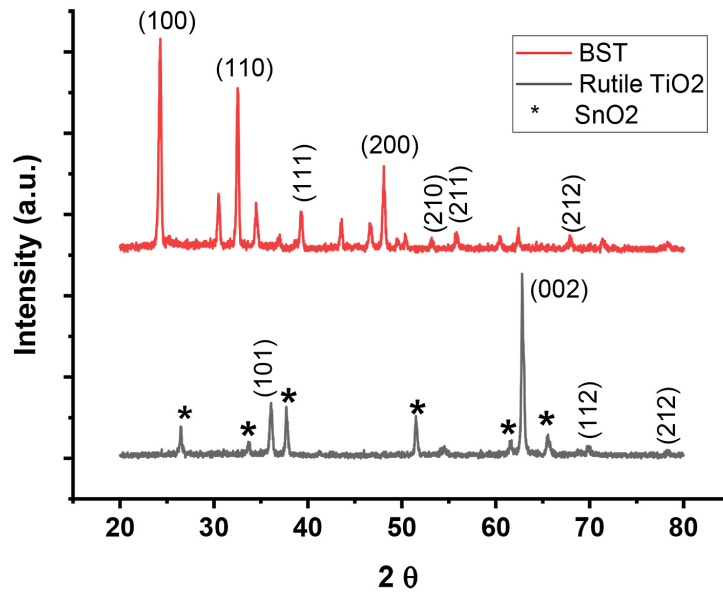


Figure 2. X-ray diffraction of Ba_{0.7}Sr_{0.3}TiO₃ fabricated on TiO₂ nanorods

calculated using the Scherrer equation as listed in Equation 1:

$$D = \frac{0.94\lambda}{\beta \cos\theta} \quad (1)$$

where: λ is the wavelength of the incident X-rays which = 0.154 nm, β is the full width at half maximum, and θ represents the diffraction angle [40, 41]. The XRD results are listed in Table 1.

Figure 3 shows FESEM pictures of the top view of Ba_{0.7}Sr_{0.3}TiO₃ nanorods prepared using the hydrothermal method on a TiO₂ substrate at

150 °C for 2 hours. The TiO₂ nanorods were previously produced on an FTO substrate. Figure 3 shows the FE-SEM images of the surface of BST thin films, which primarily represent the morphology of the top layer and data on particle size, shape, and size distribution and also shows typical FESEM images of the morphology of BST films and cross-section view. Rutile TiO₂ and FTO have almost equal lattice constants, which permit the epitaxial growth of TiO₂ on the FTO film enabling the rods to grow. The images reveal that the BST nanorod arrays grow uniformly on the TiO₂ substrate. The top view shows that the

Table 1. Experimental results of XRD data for Ba_{0.7}Sr_{0.3}TiO₃

Ba _{0.7} Sr _{0.3} TiO ₃	2θ (degree)	hkl	β (degree)	Crystallite size (nm)	a=b (nm)	c (nm)
	24.2968	100	0.30340	26.79	0.366	0.376

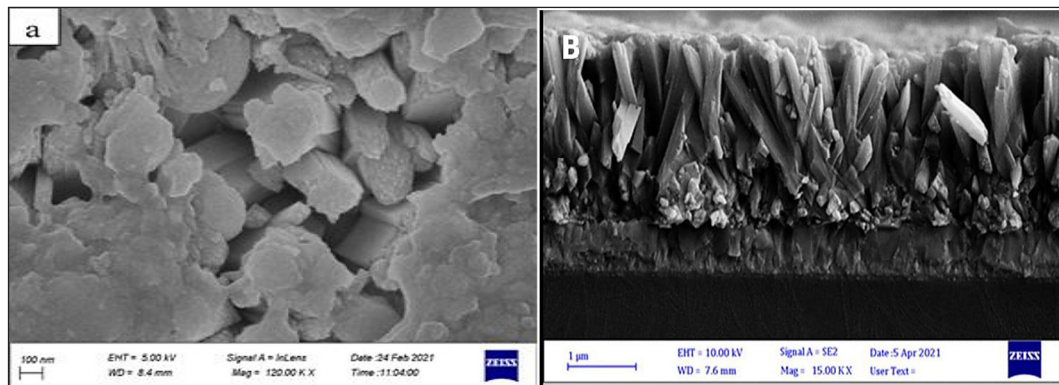


Figure 3. FESEM images of Ba_{0.7}Sr_{0.3}TiO₃ nanorods (a) the top view (b) cross section

nanorods are nearly perpendicular to the TiO₂ substrate. The nanorods are tetragonal in shape with square top facets [42]. As shown in Figure 3, some of the NRs are inclined while others are standing vertically on the titanium oxide film as their lengths reached approximately 2.360 μm, while their diameter was 202.59 nm [43].

Figure 4 shows the photoluminescence spectra (PL) of Ba_{0.7}Sr_{0.3}TiO₃ nanorods prepared using the hydrothermal method at 150 °C for 2 h. The BST film obtained was excited by 285 nm wavelength. A strong luminescent band centered at 367 nm (3.37eV) was detected and the measurements were implemented at ambient temperature. From the observation of the PL spectra, the band peaks due to oxygen vacancies and radiative transformations inside the sub-states started from the Ba_{0.7}Sr_{0.3}TiO₃ surface are in charge of these emissions [32, 44–46]. Figure 5 reveals

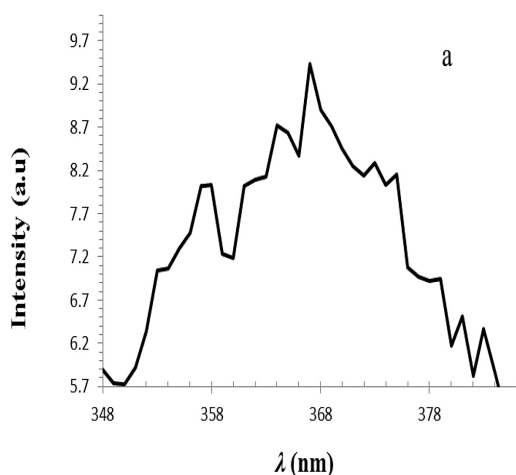


Figure 4. PL spectra of Ba_{0.7}Sr_{0.3}TiO₃ NRs

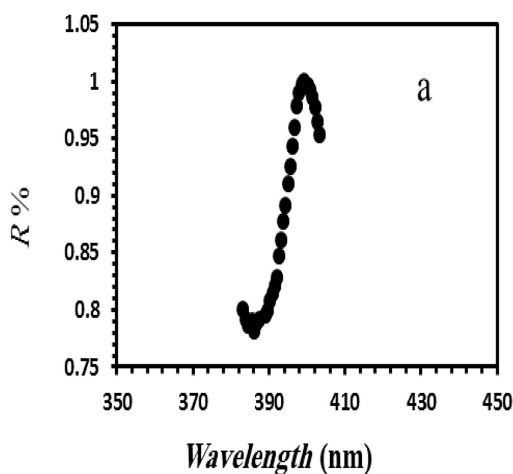


Figure 5. Diffuse reflectance spectra of the Ba_{0.7}Sr_{0.3}TiO₃ film

the diffuse reflectance spectra of Ba_{0.7}Sr_{0.3}TiO₃ ceramics in the range of 300–420 nm, and Figure 6 shows the discovered optical band values for Ba_{0.7}Sr_{0.3}TiO₃ ceramics with various periods of time. The energy gap value was deduced by utilizing reflection data; the optical band gap energy (E_{gap}) was computed using Kubelka and Munk's equation. The Kubelka-Munk equation is as follows:

$$F(R_{\infty}) = \frac{(1-R_{\infty})^2}{2R_{\infty}} = \frac{K}{S} \quad (2)$$

where: $F(R_{\infty})$ is the Kubelka-Munk function or the absolute reflectance of the sample, S is the scattering coefficient, can be used to link the absorption coefficient (K) to reflectance (R).

All light will be transmitted or absorbed if S approaches zero (no scattering), while all light will be reflected if K approaches zero (no absorption). Figure 6 show the absorption spectra translated from diffuse reflectance using the Kubelka-Munk function $F(R)$. As shown in Figure 6, the energy band gap (E_g) for the prepared samples is 3.13 eV [47–51].

For BST nanorod films with various concentrations, the DC conductivity $\ln(\sigma)$ varies as a function of $(1000/T)$ across a temperature range of 25 to 135 °C. Figure 7 shows the change of Ba_{0.7}Sr_{0.3}TiO₃ DC conductivity at 150 °C, the samples were produced using the hydrothermal technique. Using equation 3 below to estimate activation energy (E_a),

$$\sigma = \sigma^{\circ} \exp(E_a/kT) \quad (3)$$

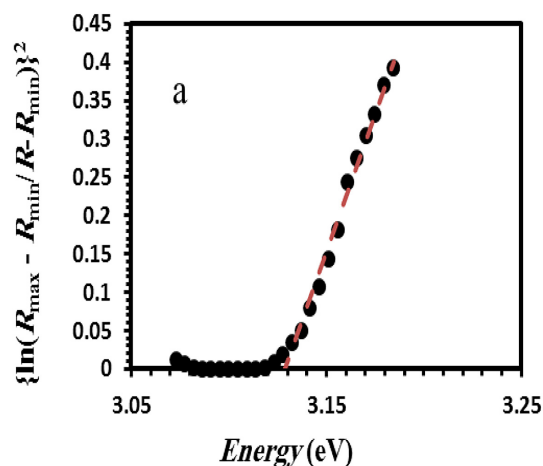


Figure 6. UV-Vis diffuse reflectance spectra of the Ba_{0.7}Sr_{0.3}TiO₃ film

where: σ , σ° , k , and T are the conductivity, constant, Boltzmann constant, and absolute temperature respectively.

The activation energy was calculated from Figure 7 and was equal to 0.15804 eV. The sample conductivity increases along with temperature up to a point termed the Curie temperature, at which the material transitions from the ferroelectric to the paraelectric state. This illustrates the impact of the conduction process on the electric dipole moment. Conductivity drops dramatically at elevated temperatures owing to the existence of free electrons that are thermally activated. Conductivity between Ba and Sr at low temperatures

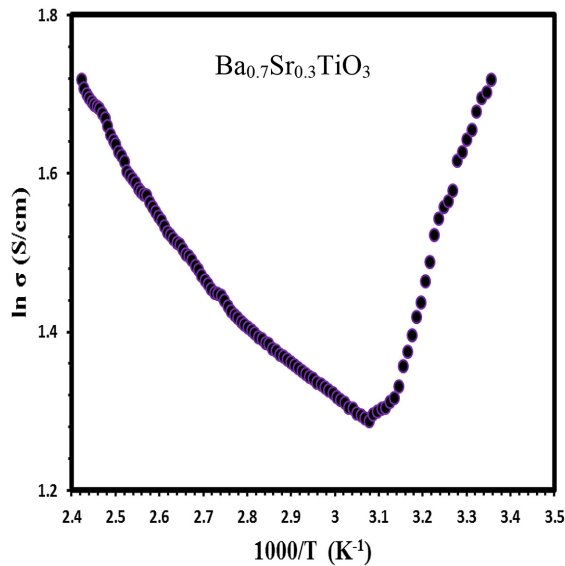


Figure 7. DC conductivity of the Ba_{0.7}Sr_{0.3}TiO₃ film

follows the polaron hopping hypothesis. The activation energies estimated in the ferroelectric area confirm the existence of the polaron hopping model. Conductivity in the ferroelectric zone is not reliant on electron concentration, but rather on thermal activation of mobility.

Figure 8 shows the J-V curve for SS-DSSC based on BSTNR film and Figure 9 shows the power of the solar cell as a function of voltage. The short circuit photocurrent density (J_{sc}), open circuit voltage (V_{oc}), FF, and overall energy conversion efficiency have been deduced from Figures 8 and showed a 35.38 mA/cm², 0.57 V, 0.353, and 0.071 respectively. The reason for the low cell efficiency is the low current density, whereby the chances of electrons reaching the FTO are few, which promotes the occurrence of the recombination process. Although the BST film was hydrothermally treated in order to enhance the bonding between the nanoparticles and reduce the recombination process, the current density was relatively low, which led to low efficiency. The thickness of the BST film in the form of nanorods was close to 2 micrometers, as shown in Figure 3, as the increase in the surface area exposed to light leads to an increase in the number and length of nanorods in order to ensure and gain more incident light, which in turn is responsible for the generation of photoexcited electrons, constituting one of the important factors to increase the current density. The behavior of electron lifetime (τ_n) showed using an open circuit voltage decay (OCVD) experiment. The OCVD technique was used to determine τ_n of the

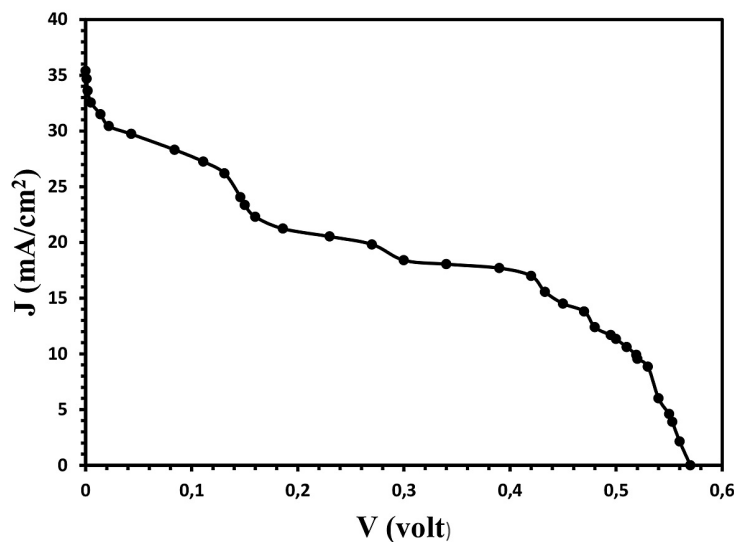


Figure 8. J-V curve for DSSC based on BSTNRs

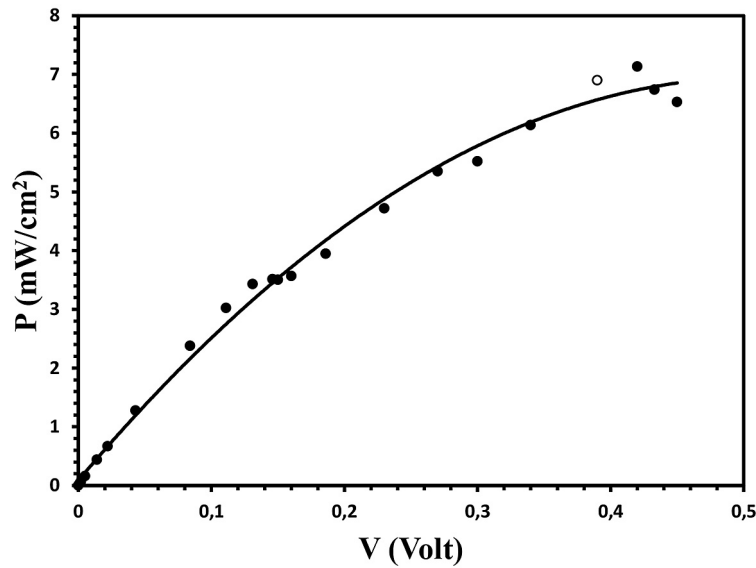


Figure 9. Power of the solar cell as a function of voltage

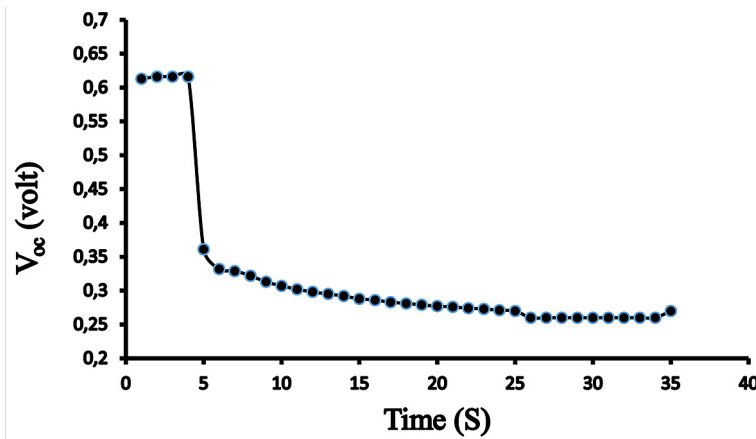


Figure 10. Open circuit voltage decay of Ss-DSSCs

minority charge carriers, where the observed decay in the open circuit voltage is monitored by equipping the cell with a current pulse, and then the lifetime is calculated using the following expression [52–54]:

$$\tau_n = -\frac{k_B T}{q} \left(\frac{dV}{dt} \right)^{-1} \quad (4)$$

where: V and T are the voltage and temperature respectively.

The OCVD of BST films electrode-based ss-DSSCs is seen in Figure 10 where the voltage decay is inversely varied with τ_n . Figure 10 also showed that the V_{oc} started with 0.61 V and then begins to sharply decay, indicating the process of recombination. The faster response of OCVD may be due to the low concentration of electrons that set the recombination process.

CONCLUSIONS

The hydrothermal technique has applied at 150 °C for 2 hours to fabricate polycrystalline perovskite $Ba_{0.7}Sr_{0.3}TiO_3$ samples. The absence of any TiO_2 peaks in the XRD patterns of the samples shows that the materials have been fully transferred to the BST. The broadband of BST film that appeared in the photoluminescence spectra was indicative of a relaxation occurring by several pathways. UV-Vis spectra demonstrate that the replacement between Ba^{2+} by Sr^{2+} showed a decline in the value of E_g , which can be attributed to the presence of an intermediate energy level located within the band gap of the BST film. An I_{sc} , V_{oc} , FF, and efficiency of solid-state dye-sensitized solar cells based on prepared BST film have been measured and the efficiency was 0.071.

REFERENCES

1. Setter N., and Damjanovic D. Ferroelectric thin films: Review of materials, properties, and applications. *Appl. Physics*. 2006; 100-051606, <https://doi.org/10.1063/1.2393042>.
2. Cao, W.Q., F.L. Li, M.M. Ismail and G. Xiong. Dielectric properties of Y_2O_3 and Nb_2O_5 Co-doped barium titanate ceramics. *Jpn. J. Appl. Phys.* 51 041503.2012; <https://doi.org/10.1143/JJAP.51.041503>
3. Cao, W.Q. and M.M. Ismail. Giant dielectric constant phenomena in Bi_2O_3 -doped $Ba_{0.8}Sr_{0.2}TiO_3$ ferroelectrics. *Mater. Technol.* 2017; 32: 321–326, <https://doi.org/10.1080/10667857.2016.1216297>.
4. Al-Sarraj Z.S.A., Ismail M.M., Ali S.M. and Cao W.Q. Structural Characterization of Nano-Crystalline $BaTiO_3$ Powder Prepared Using Hydrothermal Method. *J. Adv. Mater. Res.* 2011; 324: 205–208. <https://doi.org/10.4028/www.scientific.net/AMR.324.205>.
5. Cao W.Q., Xu L.F., Ismail M.M., Huang L.L. Colossal dielectric constant of $NaNbO_3$ doped $BaTiO_3$ ceramics *J. Mater. Sci-Poland.* 2016; 34, 322–329, <https://doi.org/10.1515/msp-2016-0065>.
6. Ismail M.M. Ferroelectric characteristics of Fe/Nb co-doped $BaTiO_3$ *J. Mod. Phys. Lett.* 2019; 33: 1950261, <https://doi.org/10.1142/S0217984919502610>.
7. Singh B.S., Sharma B.H., Sarma K.N.H., Phanjoubam S. Structural and optical properties of barium Strontium titanate ($Ba_{0.5}Sr_{0.5}TiO_3$) thin films. *Ferroelectric Lett Sect.* 2006; 33: 83–90, <https://doi.org/10.1080/07315170600870659>.
8. Iskandar J., Syafutra H., Juansah J., Irzaman. Characterizations of Electrical and Optical Properties on Ferroelectric Photodiode of Barium Strontium Titanate ($Ba_{0.5}Sr_{0.5}TiO_3$) Films Based on the Annealing Time Differences and its Development as Light Sensor on Satellite Technology. *J. Proc. Environ. Sci.* 2015; 24: 324–328, <https://doi.org/10.1016/j.proenv.2015.03.042>.
9. Khare A., Chauhan N. The effect of Mg doping on structural and luminescent properties of Barium Strontium Titanate (BST). *J. Phys. Procedia.* 2015; 76: 86–91, <https://doi.org/10.1016/2015.10.016>.
10. Dhumal G.S., Kulkarni B.S., Jayasingh E.M., Joshi B.P., Salunkhe J.D. Effect of cobalt doping on structural, dielectric and magnetodielectric properties of $Ba_{0.95}Sr_{0.05}TiO_3$ ceramics. *J. Mater. Sci: Mater. Electron.* 2015; 27: 1421–1426, <https://doi.org/10.1007/s10854-015-3906-2>.
11. Attar S.A., Sichani S.E., Sharafi S. Structural and dielectric properties of Bi-doped barium strontium titanate nanopowders synthesized by sol–gel method. *J. mater. Res. Technol.* 2017; 6: 108-115, <https://doi.org/10.1016/J.JMRT.2016.05.001>.
12. Singh B.S., Sharma B.H., Sarma K.N.H., Phanjoubam S. Optical and structural properties of nano-sized barium strontium titanate ($Ba_{0.6}Sr_{0.4}TiO_3$) thin film. *Mod. Phys. Lett. B.* 2008; 22: 693-700, <https://doi.org/10.1080/073151706008706598>.
13. Lee Y.D., Lee H.K., Lee H.M., Cho I.N., Kim Y.B. Synthesis of electrospun $BaSrTiO_3$ /PVP. Nanofibers. *J. Sol-Gel Sci Technol*, 2010; 53: 43–49, <https://doi.org/10.1007/s10971-009-2054-7>.
14. Ramadass N. ABO₃-Type Oxides - Their Structure and Properties -- A Bird's Eye View. *Mater. Sci. Eng.* 1978; 36: 231–239, [https://doi.org/10.1016/0025-5416\(78\)90076-9](https://doi.org/10.1016/0025-5416(78)90076-9).
15. Kaur A, Singh L, Asokan K. Electrical relaxation and conduction mechanisms in iron doped barium strontium titanate. *Ceram. Int.* 2018; 44: 3751–3759, <https://doi.org/10.1016/j.ceramint.2017.11.15>.
16. Gao L., Guan Z., Huang S., Liang K., Chen H., Zhang J. Enhanced dielectric properties of barium strontium titanate thin films by doping modification. *J. Mater. Sci: Mater. Electron.* 2019; 30: 12821–12839. <https://doi.org/10.1007/s10854-019-01670-w>
17. Wang Y., Chen W., Wang B., Zheng Y. Ultrathin Ferroelectric Films: Growth, Characterization, Physics and Applications. *J. Mater.* 2014; 7: 6377–6485. <https://doi.org/10.3390/ma7096377>.
18. Salman N.O., Ahmed S.D., Abed L.A., Dawood O.M. Preparation pure ZnO, La-doped ZnO nanoparticles using sol-gel technique: Characterization and Evaluation Antibacterial Activity. *Iop conf. ser. mater. sci. eng.* 2019; 1–9. <http://dx.doi.org/10.1088/1757-899X/518/3/032012>.
19. Shaban N., Bahar M. Synthesis and Characterization of Fe and Ni Co-Doped $Ba_{0.6}Sr_{0.4}TiO_3$ Prepared by Sol-Gel Technique. *J. Theor. Comput. Sci.* 2017; 4: 1–6. <https://doi.org/10.4172/2376-130x.1000157>.
20. Iskandar J., Jenie P.R., Siregar J.U., Yulianto B., Irzaman. Application of thin film barium strontium titanate (BST) in a microcontroller based tool to measure oxygen saturation in blood. *Ferroelectrics*, 2020; 554: 134–143. <https://doi.org/10.1080/00150193.2019.1684755>.
21. Reddy N.I., Reddy V.C, Cho G.M, Shim J. Morphological and chemical structure of silver-doped barium strontium titanate thin films fabricated via pulsed laser deposition. *Mater. Res. Express* 2017; 4: 1–12. <https://doi.org/10.1088/2053-1591/aa7c6d>.
22. Palupi K.E., Irzaman, Alatas H., Yulianto B., Umam R., Andriana B.B., Sato H. Analysis of Spectroscopy: Mustard Greens Leaf of Chlorophyll as a $Ba_{0.2}Sr_{0.8}TiO_3$ (Barium Strontium Titanate) Film Dopant. *Integrated Ferroelectrics*, 2019; 201: 75–85, <https://doi.org/10.1080/10584587.2019.1668692>.

23. Irzaman, Dahrul M., Yuliarto B., Hammam A.K., Alatas H. Effects of Li and Cu dopants on the crystal structure of $Ba_{0.65}Sr_{0.35}TiO_3$ thin films. *Ferroelectrics Letters*, 2018; 45: 49–57. <https://doi.org/10.1080/07315171.2018.1537333>.
24. Shen Y.Z, Wang Y., Tang Y., Yu Y., Luo Q.W., Wang X., Li Y., Wang Z., Song F. Glass modified barium strontium titanate ceramics for energy storage capacitor at elevated temperatures. *J. Materiomics*, 2019; 5: 641–6482. <https://doi.org/10.1016/j.jmat.2019.06.003>.
25. Irzaman, Putra R.I., Aminullah, Syafutra H., Alatas H. Development of ferroelectric solar cells of barium strontium titanate ($Ba_xSr_{1-x}TiO_3$) for substituting conventional battery in LAPAN-IPB Satellite (LISAT). *Procedia Environmental Sciences*, 2016; 33: 607–614. <https://doi.org/10.1016/j.proenv.2016.03.114>
26. Enhessari M., Parviz A., Ozaee K., Abyaneh H.H. Synthesis and characterization of barium strontium titanate (BST) micro/nanostructures prepared by improved methods. *Journal of Nano Dimension*, 2011; 2: 85–103. <https://doi.org/10.7508/ijnd.2011.02.001>
27. Cao W.Q., Li F.L., Ismail M M and Xiong G. Dielectric Properties of Y_2O_3 and Nb_2O_5 Co-Doped Barium Titanate Ceramics, *Jpn J Appl Phys*, 2012; 51: 041503. <https://doi.org/10.1143/jjap.51.041503-5>.
28. Rashad M.M., Turkey O.A., Kandil T.A. Optical and electrical properties of $Ba_{1-x}Sr_xTiO_3$ nanopowders at different Sr^{2+} ion content. *J. Mater. Sci: Mater. Electron*. 2013; 24: 3284–3291. <https://doi.org/10.1007/s10854-013-1244-9>
29. Goud P.J., Alkathy S.M., Sandeep K., Ramakanth S., Raju J.C.K. Influence of laser fluence on structural, optical and microwave dielectric properties of pulsed laser deposited $Ba_{0.6}Sr_{0.4}TiO_3$ thin films. *J. Mater. Sci: Mater. Electron*. 2018; 29: 15973–15982. <https://doi.org/10.1007/s10854-018-9683-y>.
30. Podhorodecki A., Gaponenko V.N., Banski M., Rudenko V.M., Khoroshko S.L., Sieradzki A., Misiewicz J. Green emission from barium–strontium titanate matrix introduced into nano-porous anodic alumina. *Optical Materials*, 2012; 34: 1570–1574. <http://dx.doi.org/10.1016/j.optmat.2012.03.025>.
31. Wu A., Vilarinho M.P., Gonza'lez M. Synthesis and characterization of barium strontium titanate nano powders by low temperature ambient pressure sol process. *J Nanopart Res*, 2010; 12: 2221–2231. <https://doi.org/10.1007/s11051-009-9788-6>.
32. Liu J., Wu D., Deng Y., Li A., Ming N. Structure and Properties of Barium Strontium Titanate Nanoparticles Synthesized by a Hydrothermal Method. *Integrated Ferroelectrics*, 2006; 78: 289–297 <http://dx.doi.org/10.1080/10584580600663441>.
33. Zhao Y., Gu X., Qiang Y. Influence of growth time and annealing on rutile TiO_2 single-crystal nanorod arrays synthesized by hydrothermal method in dye-sensitized solar cells. *Thin Solid Films*, 2010; 520: 2814–2818. <http://dx.doi.org/10.1016/j.tsf.2011.12.055>.
34. Salman O.N., Agool I.R., Ismail M.M. Preparation of the scattering layer based on TiO_2 nanotube and their dye sensitized solar cell applications. *Appl. Phys. A*. 2017; 123: 402. <https://doi.org/10.1007/s00339-017-1012-4>.
35. Chen Y., Zhang L., Zhang Y., Gao H., Yan H. Large-area perovskite solar cells – a review of recent progress and issues. *RSC Adv*. 2018; 8: 10489–10508. <https://doi.org/10.1039/c8ra00384j>.
36. Dewi R. Optical characterization of $Ba_{1-x}Sr_xTiO_3$ thin film properties using ultraviolet-visible spectroscopy. *AIP Conference Proceedings*, 2020; 2219: 040001-6. <https://doi.org/10.1063/5.0003054>.
37. Joshi A.U., Lee S.J. Template-Free Hydrothermal Synthesis of Single-Crystalline Barium Titanate and Strontium Titanate Nanowires. *Small*, 2005; 12: 1172–1176. <http://dx.doi.org/10.1002/smll.200500055>.
38. Salman O.N., Ismail M.M., Ali T.H. Growth Time Influence on Optical and Electrical Properties of TiO_2 Nanorods Prepared via Hydrothermal Method. *J. Phys. Conf. Ser.* 2021; 2114: 012063. <https://doi.org/10.1088/1742-6596/2114/1/012063>.
39. Jasim A.S., Salman O.N. Hydrothermally native defect induced transparent p-n TiO_2 homojunction diode. *Opt Quant Electron*, 2023; 55: 702, 59–69. <http://dx.doi.org/10.1007/s11082-023-04984-6>.
40. Yousif N.A., AL-Jawad S.M.H., Taha A.A. Preparation and Characterization of Pure and Ni/Co–Co-doped Fe_3O_4 Nanoparticles and Investigation of Their In Vitro Hemolysis Effects. *Plasmonics*, 2023; 19: 2345–2361. <https://doi.org/10.1007/s11468-023-02167-3>.
41. Yousif N.A., AL-Jawad S.M.H. Influence of Laser wavelength on morphological and optical of properties ZnO nanoparticles prepared by laser ablation in water, *J. Phys.: Conf. Ser.* 2021; 1795 012056. <https://doi.org/10.1088/1742-6596/1795/1/012056>.
42. Dong H., Lu G., Jin D., Chen J., Cheng J. Enhanced tunability of sandwich-like structural barium strontium titanate thin films on stainless steel substrates. *J. Mater Sci*, 2016; 51: 8414–8421. <https://doi.org/10.1007/s10853-016-0093-3>.
43. Cao C., Hu C., Wang X., Wang S., Tian Y., Zhang H. UV sensor based on TiO_2 nanorod arrays on FTO thin film. *Sensors and Actuators B*, 2011; 156: 114–119. <http://dx.doi.org/10.1016/j.snb.2011.03.080>.
44. Wu J.Y., Wang N., Wu Y.S., Chen M.X. Transparent Barium Strontium Titanate Ceramics Prepared by Spark Plasma Sintering. *J. Am. Ceram. Soc*, 2011; 94(5): 1343–1345. <https://doi.org/10.1111/j.1551-2916.2011.04507.x>.
45. Orhan E., Pontes M.F., Pinheiro D.C., Longo E., Pizani S.P., Varela A.J, Leite R.E, Boschi M.T.,

- Beltran A., Andres J. Theoretical and experimental study of the relation between photoluminescence and structural disorder in barium and strontium titanate thin films. *J. Eur. Ceram. Soc.* 2005; 25: 2337–2340. <https://doi.org/10.1016/j.jeurceramsoc.2005.03.053>
46. Salman N.O., Dawood O.M., Ali K.A., Ahmed S.D., Hassoon I.K. Low cost synthesis of ZnO nano thin films by electrochemical deposition. *Digest Journal of Nanomaterials and Biostructures*, 2017; 12: 719–726.
47. Samantaray B.C., Goswami N.L.M., Bhattacharya D., Ray K.S., Acharya N.H. Photoluminescence of properties Eu³⁺-doped barium strontium titanate (Ba, Sr) TiO₃ ceramics. *Mater. Lett.* 2004; 58: 2299–2301. <http://dx.doi.org/10.1016/j.matlet.2004.03.001>.
48. Ghosh K.S., Rout K.S., Tiwari A., Yadav P., Sczancoski C.J., Filho R.G.M., Cavalcante S. L. Structural refinement, Raman spectroscopy, optical and electrical properties of (Ba_{1-x}Sr_x)MoO₄ ceramics. *J. Mater. Sci: Mater. Electron.* 2015; 26: 8319–8335. <http://dx.doi.org/10.1007/s10854-015-3498-x>.
49. Kavitha V., Mayandi J., Mahalingam P., Sethupathi N. Optical and structural properties of tungsten-doped barium strontium titanate. *Materials Today: Proceedings*, 2020; 23: 12–15. <http://dx.doi.org/10.1016/j.matpr.2019.05.351>.
50. Sami T.A., Salman N.O., Ismail M.M. Ferroelectric Photodiode Based on BaTiO₃ Nanorods Film. *J. Phys.: Conf. Ser.* 2021; 1795: 12047–13. <http://dx.doi.org/10.1088/1742-6596/1795/1/012047>.
51. Ismail M.M., Salman O.N., Ali T.H. Effect of TiO₂ nanorod thickness on optical properties of Ba_{0.8}Sr_{0.2}TiO₃ film via hydrothermal method, *J. Solid State Electrochemical*, 2021; 25: 2429–2441. <https://doi.org/10.1007/s10008-021-05022-9>.
52. Salman O.N, Ismail M.M., Dawood M.O. Porous BaTiO₃ film for dye-sensitized solar cells. *Opt Quant Electron*, 2023; 55, 469. <https://doi.org/10.1007/s11082-023-04741-9>.
53. Husam N., Odai N. Salman O.N., Ismail M.M. Influence of NaOH Concentration on Structural, Morphological, Optical, and Electrical Characterization of Perovskite Sodium Bismuth Titanate Prepared by Hydrothermal Method ECS. *J. Solid State Sci. Technol*, 2024; 13: 043009. <https://doi.org/10.1149/2162-8777/ad3d08>.
54. Nahedh H., Salman O.N., Mukhlis M. Ismail. Performance of dye-sensitized solar cells of perovskite sodium bismuth titanate layer and studying the effect of Fe-doped on the photovoltaic properties. *J. Appl. Phys. A*, 2024; 130, 843, 1–14. <https://doi.org/10.1007/s00339-024-07998-3>.